IMPLEMENTATION OF A GRAVITY COMPENSATING MIRROR ON A LARGE APERTURE ANTENNA

R. Bruno, W. Imbriale, and M. Moore
Jet Propulsion 1 Amatory, California Institute of Technology
Pasadena, California

S. Stewart
PRC, inc.
Pasadena, California

ABSTRACT

A proposed technique for compensating gravity - induced structural deformations on the main reflector of a large aperture antenna is to utilize a deformable flat plate (1 DFP) installed at onc of the mirror locations in the beam waveguide optics. An initial 1ow-cosI demonstration of the technique was performed at a 34-meter beam waveguide (BWG) antenna using a fixed elevation angle. and a manually adjustable DFP with 49 regularly spaced actuators. The effective RMS surface error was improved from 0.59 mm for the initial no-correction flat plate 10 0.49 mm for the initial analytically-derived correcting surface, and finally, m 0.36 mm for the hologmphy-derived DFP. This would rcprc.sent a gain improvement of approximately 2.0 dB at 32 GHz. An automated DFP with 16 actuators in optimized locations has 1 ·een assembled with a mirror surface RMS that measures within 0.28 mm of the required compensating surface.

INTRODUCTION

At the NASA Deep Space Network (DSN) Goldstone Complex, located in the Mojave Desert in California, a 34-meter-diamet er BWG antenna (DSS-13) has become an integral part of an advanced systems program and a test bed for technologies being developed to introduce Ka-band (32-GHz) frequencies into the DSN. A BWG feed system is composed of onc or more feedhorns with a series of flat and curved mirrors arranged so that power can be propagated from the horn through the mirrors with minimum losses. Horns and equipment can be located in a large stable enclosure at an accessible location. The antenna efficiency at 34 GHz was found to depend significantly on the elevation angle, i.e.., it decreased from 45 to 35% as the elevation angle changed from 45 10 20 degrees. This elevation angle dependence is due to the deformation of the main reflector cause.(i by the resulting change in gravitational force applied to the antenna struct arc.

A proposed technique for compensating gravity-induced Structural deformations is to utilize a DFP installed at one of the mirror locations in the beam waveguide optics. An initial low cost demonstration of the technique was performed at 1) SS-13 using a fixed elevation angle and a manually adjustable DFP with 49 regularly spaced actuators. in previous DFP, the actuator locations arc typically arranged in a predetermined pattern. In this approach, the actuator locations are optimized according 10 the required contours, thus reducing the number of required actuators while maintaining the necessary level of performance. Microwave holography[1] was used at an elevation angle of 12.7-degrees to obtain a surface distortion map of the main reflc·tor: 1) with an undistorted flat plate, and 2) after the calculated correction had been applied to the DFP. Near-real-time holography was then used to adjust the surface, to obtain the lowest RMS surface error obtainable within the short time available for the experiment. The effective RMS surface error was improved from 0.59 mm for the initial no-correction flat plate to 0.49 mm for the initial analytically-derived correcting surface, and finally, to 0.36 mm for the ilo]ography-derived DFP.[2] This would re.present a gain improvement of approximately ?..0 dB at 32 GHz. This problem of elevation angle efficiency dependence aiso occurs at the NASA 70-meter antenna. Because of the larger structure, the efficiency dependence is even gi eater going from 35% at the 45-degree rigging angle to 15% at 20 degrees. As a solution for both systems, a fully actuated DFP is being designed and built. The same plate will be tested in both the 34- and 70-meter antennas. Gain improvements of 1- 2 dB arc expected for the 34-meter antenna, and more than 3 dB at low- and high-elevation angles for the 70-meter antenna.

APPROACH

The approach taken was to thoroughly test the components and assembly procedures of the planned

1)1 'P with a two-actuator fixture to verify performance and minimize risk prior LO installing the fully actuated plate on the antenna. Analysis to determine optimal actuator placement was done concurrently with the component testing with the intent of completing the analysis and the preliminary [cSting simultaneously. In this manner, the actuator location design and the hard ware selection and verification would be completed at the same time. Although this approach minimized the lime 10 development, it also meant preliminary testing was done with approximations in terms of expected loads ar Id deflection pat tern. Thus, the component testing used extremely conservative values with good results. A lab prototype utilizing the. selected hardware and assembly technique was built and tested. The data gained from the lab mode] will be used to modify modeling assumptions to provide more accurate input into the optimization program. After comparing experimental and analytical results and adjusting the analytical mode], a final actuator design will be developed for installation on the 34-meter antenna.

DEFINITION OF MIRROR CONTOUR

The primary reflector on DSN antennas is designed with a backup structure supporting reflective panels. The pane] mounts arc adjustable and typically the panel positions arc optimized, in terms of surface displacement error, with the m ain reflector at a 45-d 'gycz-elevation angle. This gives optimum antenna performance at 45°, which degrades as the elevation angle moves away from 45° due to reflector deformation from gravitational forces. The deformable mirror can c.om]m.sate for the reflector deformation by essentially correcting the path length error over the reflector surface. Thus, the desired mirror contour at a particular elevation is related 10 the deformation of the primary reflector at that setting.

The mirror contour for compensation on the 34-meter antenna was derived by analysis using measured path length errors as determined by a combination of theodolite and microwave holography measurements.

ANALYSIS FOR ACTUATOR PLACEMENT

The actuator placement is determined using a simulated annealing algorithm,[3] which can provide near optimal results with minimal computational time. As Cach new actuator configuration is considered within the optimi zation routine, the relationship between actuator travel and overall plate deformation must be evaluated. 1 lowever, the act of selecting ncw actuator locations means the structure has changed and a ncw stiffness matrix is required and a displacement solution must be calculated. To minimize computational time, Lhc structure stiffness is partitioned according to possible actuator IOc.aliens and the remaining structure. By using static condensation on the partitioned matrix, only a small subset of the full stiffness matrix undergoes repeated solving during the iterative optimization procedure.

Start with the compatibility equation, the force-displacement relationship, and the force equilibrium equation:

$$A = \beta u \tag{1}$$

$$P = K(A - \Lambda_0) \tag{?.}$$

$$F = \beta^T P \tag{3}$$

where A is the vector of element displacements in local coordinates, u is the vector of nodal displacements, 1' is the vector of element forces, K represents the assembl y of the singular element stiffness matrices, F is the vector of external nodal forces, and β relates the element local degrees of freedom (dofs) to the global degrees of freedom. In this application, Δ_0 represents the initial actuator length change. Using equation (2) in (3) and recognizing [hat F = 0, giv cs:

$$\beta^T K(\Lambda - \Lambda_0) = 0 \tag{4}$$

Usc equation (1) in (4) and solve for u to get:

$$U = K_G^{-1}\beta^T A'A_o \tag{5}$$

where K_G is the global stiffness matrix. This defines the nodal displacements in terms of the actuator initial length changes. Each time a ncw configuration of actuators is selected, K_G changes. The optimization is an iterative process requiring repeated inversion of K_G if the current form of the equations is used. The stiffness matrix, K_G, can be quilt large for a plate model wiLh enough resolution 10 provide the deformation accuracy dc.sired thus making the optimization process quite time consuming. By reordering and partitioning the matrices in equation (5), Lhc resultant matrix equation to be solved can be reduced in size.

Start by examining $\beta^T K\Lambda_0$. As shown in equation (l), β relates the element local degrees of freedom to

the global degrees of freedom. For clarity, first order the system degrees of freedom in the following manner: 1) out-of-plane dofs and 2) remaining dofs. Order the elements considered in K with actuator elements first, then plate elements. The actuator elements are rod elements with only an axial degree of freedom which points in the out-of-plane direction. The β matrix is a sparsely populated matrix with entries defined by the geometry of the system. By ordering it in the manner described, the first n_a rows, where n_a represents the number of actuators looks like:

$$\begin{bmatrix} I & 0 \end{bmatrix} \tag{6}$$

where I, the identity matrix, is n_a by n_a and the right hand side is a n_a by $(z_d + r_d)$ zero matrix where z_d is the number of out-of-plane degrees of freedom in the problem and r_d is the number of remaining degrees of freedom.

Next, consider the form of K, the element stiffness matrix. Since the equations are ordered by actuator elements first, K is constructed as follows:

$$\begin{bmatrix} K_a & 0 \\ 0 & K_R \end{bmatrix} \tag{7}$$

where K_a is the n_a by n_a matrix with diagonal entries $(AE)_i/l_i$ corresponding to the i^{th} actuator. K_R is the element stiffness matrix of the plate.

Finally, consider Λ_0, the vector of initial displacements. In this problem, the initial actuator length changes make up the first n_a entries of Λ_0 and the remainder of the vector is null. When forming $\beta^T K \Lambda_0$, the resultant vector, P^*, has non-zero entries only in the top n_a places. Therefore, equation (5) can be rewritten as:

$$K_G u = P^* \tag{8}$$

This can be partitioned into the out-of-plane degrees of freedom and the remaining degrees of freedom:

$$\begin{bmatrix} K_{G11} & K_{G12} \\ K_{G21} & K_{G22} \end{bmatrix} \begin{bmatrix} u_1 \\ u_2 \end{bmatrix} = \begin{bmatrix} P_1^* \\ P_2^* \end{bmatrix} \tag{9}$$

K_{G22} remains unchanged for all actuator locations and $P_2^* = 0$. Then

$$K_{G21} u_1 + K_{G22} u_2 = 0 \tag{10}$$

and

$$u_2 = -K_{G22}^{-1} K_{G21} u_1 \tag{11}$$

Using equation (11) in the top set of equations in equation (9), gives

$$\begin{aligned} \left(K_{G11} - K_{G12} K_{G22}^{-1} K_{G21}\right) u_1 &= P_1^* \\ K_R u_1 &= P_1^* \end{aligned} \tag{12}$$

where K_{G22} need only be inverted once. More importantly, since K_{G11} is the only term affected by the actuator locations the reduced matrix, K_R can be modified directly as actuator positions are changed.

Solve for u_1 and express as:

$$u_1 = S P_1^* \tag{13}$$

in equation (13), P_1^* is a ndof length vector with non-zero entries at the degrees of freedom corresponding to the actuator positions. Then the actuator induced shape will be

$$u_g = S_a P_a^* \tag{14}$$

where S_a contains the n_a columns of S corresponding to the non-zero entries P_a^*, is the non-zero portion Of P^*. Let the desired shape be u_d. For the best fit to u_d, minimize the error between the desired shape and the actuator induced shape, u_g. The objective function in the optimization routine is

$$\min J = \left(U_d - u_g\right)^T \left(u_d - u_g\right) \tag{15}$$

Minimizing with respect to P_a gives

$$P_a = \left(S_a^T S_a\right)^{-1} S_a^T u_d \tag{16}$$

Using this formulation, the steps necessary at each iteration are:

1) Select actuator locations

2) Add the actuator stiffnesses into K_G

3) Formulate S_a

4) *Solve* for Pa

5) Calculate u_g, J

The physical constraints of the hardware, such as minimum spacing between actuators, maximum actuator travel, and maximum actuator force are included as constraints in the optimization routine.

HARDWARE REQUIREMENTS AND SELECTION

The design criteria used for hardware selection were that it must meet the contour requirements, be reliable, and be cost effective. A test program was implemented to assure the first two requirements. Use of proven, off the shelf components further supports the last two requirements. A two station (two actuators) device was used for initial testing because it is easier to modify, provides the necessary data, and in the event of a failure offers less financial exposure to the program than does testing on the final sixteen-station device.

The actuator chosen consists of an AC stepper motor, driving a JPL designed double screw-thread final stage through a gearhead reduction. The double screw thread final output supports the reflective surface and reacts side loads without putting the motor output shaft in bending, which could cause the motor to stall.

The mirror surface selection is based on the deformation requirements as well as RF (radio frequency) considerations. The material properties and sheet thickness are chosen to avoid a "tent pole" effect around the actuators while minimizing the axial and lateral forces on the actuators.

The actuator attachments to the plate, are limited to methods that would not introduce any discontinuities on the front surface of the plate which would degrade the RF performance. Adhesive bonding was selected to reduce surface deformation that can be generated by welding. The adhesive bonding process was approached cautiously, since an earlier experiment hart unexplained beading failures.

Hardware Description

There are four significant components in the mirror:

1) Reflective surface

2) Actuator and drive motors

3) Position feedback system

4) Motor controller

These components are described below.

Reflective Surface and Attachment

The thickness and alloy of the reflective plate were the first design criteria to be determined. A thicker aluminum surface would require higher actuator forces to deflect the plate into the desired contour. Also, higher stresses would be induced in a thicker mirror for a given contour compared to a thinner plate. The bending stress must be kept well below the yield strength of the material to ensure neither permanent deformation, nor fatigue failure, since the mirror will eventually cycle through a family of contours as the antenna primary reflector rotates about the elevation axis during a tracking operation. A thinner material would have lower bending stresses and lower actuator forces, but would be more likely to undergo a "tent pole" effect where the deflections caused by the actuators are highly localized, generating a surface with distinct areas of displacement instead of a smooth contour. Given these constraints, the reflective surface, or mirror, was selected to be a 0.68-m (27-in.) diameter, 25.4-mm-thick (0.040-in.) 6000-series aluminum sheet.

A reliable method of attaching #6-32 studs to the backside of the reflective surface was another issue to be investigated. The following parameters needed to be determined: 1) bond area, 2) bonding adhesive, and 3) strength of joint, including fatigue life. The larger the bonding area on the top of the screw, the lower the adhesive stress level and the greater the fatigue strength. But a larger bonding area would also create a larger "flat spot" on the surface; from an RF viewpoint, a smaller bond area was better.

Earlier approaches used mechanical fastenings (commercially available "Pem Studs"), which worked reasonably well but produced some local surface distortion. There were also areas of high stress, which may have been a precursor to fatigue failure. Therefore, it was decided to create a flat surface on the head of a

#6-32 screw by installing a precision countersunk washer to the flat head screw and securing it with Loctite and a nut. The flat screw head and washer were adhesive-bonded to the back of the reflective surface, A 12.7-mm-diameter (0.5 -in,) precision aluminum bonding area was selected to provide an adequate bond area without creating too large of a "flat spot". The adhesive selected was Hysol EA9309.3NA, an adhesive with a high shear and peel strength with aluminum; this adhesive has been used successfully on previous tasks. Although more advanced adhesives were considered, the decision to usc the Hysol EA9309.3NA was prompted by the advantages of using a familiar product which had a sufficient load margin. Destructive testing of the joint was carried out to validate this decision.

Actuator and Drive Motors

The actuator is a JPL unique design. The criteria guiding the actuator design included: 1) required actuator stroke, 2) required actuator force, 3) motor size and speed, and 4) actuator speed. The maximum required actuator stroke was defined as 6.35 mm (0.25 in,) at the mirror surface with accuracy to within 0.02S4 mm (0.001 in.). In addition, the design needed to achieve these two objectives while minimizing the movement at the far end of the actuator so that the overall depth of the mirror assembly was not excessive. The installation on the 34-m antenna requires that the entire mirror assembly rotate. The 70-m installation is space constrained. An increase in the assembly depth complicates the positioning and/or rotation of the mirror,

After test verification of the spring rate of the mirror, the highest gear ratio (1 O: 1) for the smallest available Industrial Drives Corporation stepper motor was selected (IDC Size 12). The size of the motor-gearhead was kept as small as possible to minimize weight. The gearhead ratio was selected to be as high as possible and provide sufficient speed to maintain the required contour al all elevations during a track without lag. This high ratio maximizes the output torque from the gearhead. The final speed of the panel actuator is approximately 2..54 mm/s (O. 1 in./s).

The JPL-designed portion of the actuator converts rotary motion to linear motion through a compound screw arrangement with an effective pitch of 53 turns per inch of travel. This combination provides a stall force of 55.08 N (245 lbs). Assuming a peak mirror force of 1.35 N (6 lbs), this is a margin of approximately 40:1 against stalling the actuator in normal operat ion. During testing it was discovered that proper lubrication of the screw threads in the JPL actuator is critical, and design adjustments were made accordingly.

The actuator is attached to the reflective surface with a #6-32 stud, which fits into a bushing that is coaxially threaded with a #6-32 internal screw thread and a 7/16-2.0 external thread. The bushing also has a hex shape on one, end that fits into a coupling which has a broached hexagonal (internal) hole into which the hexagonal end of the inner bushing fits. The coupling is attached to the output end of the commercial gearhead stepper motor. The 7/1 6-20 threaded bushing fits into another internally threaded bushing that attaches to the driving base of the mirror. This attachment design allows the actuator to accommodate a shear load; this is unusual for a small actuator.

The position feedback system is provided by Lucas-Schaevitz Linearly Variable Displacement Transducers (LVDT's) to obtain a direct measurement of the actuator travel without depending on counting motor steps or monitoring the number of steps commanded. The motor controller is a commercially available unit.

TEST PROCEDURE AND RESULTS TO DATE

Bonded Joint Load Capacity

Test panels tailored to allow usc of existing fixtures were fabricated using the selected adhesive, Hysol EA 9309.3NA. Since the test fixture was restricted to a 101.6 mm by 101 .6-mm (4-in. by 4-in.) specimen, forces applied to the test panel would result in less deflection than expected in the large.r 14-station panel under a comparable load. With lcss deflection, there would be less slope at the edge of the bond. Therefore, in order to sufficiently test peel Characteristics, test material thicknesses were selected to allow the same slope at the edge of the test panel bond as the slope at the edge of the actual mirror bond. Test strengths of 59.6 N (265 lbs) minimum were obtained. Assuming a maximum mirror force of 1.35 (6 lbs), a margin of over 40:1 against failure is achieved.

Required Joint Force

A stroke of ± 6.35 mm (0.?5 in.) was assumed. This was determined from the RF analysis of required mirror shapes. The maximum calculated value was ± 0.125 in. A factor of 2 margin of safety should be more than sufficient for both mechanical and RF consideration. A two station test fixture was built and a mirror was installed, complete with attachment fixture and hold-downs. By using a piezo-crystal load cell and a dial indicator, it was possible to deflect the mirror by the

required amount to measure the force which would be on the actuator. By knowing this spring rate and using the assumed maximum deflection, a force was identified as a maximum operational force: 1.35 N (6 lbs) at 6.35 mm (0.25 in.).

Output Force Capacity of the Actuator

Using the same two-station test fixture, the spring rate of the attachment location was first measured. Then deflection was measured as the actuator drove the mirror 10 extremes of travel. These measurements were used to validate the force.

Fatigue Strength

Before the actuator design was finalized, the device was programmed and allowed to operate for a number of cycles. The stroke of the actuator was increased in five stages, beginning with ± 0.050 inches for the equivalent of 199 years of operation, up to ± 0.250 inches for 11.3 years of equivalent life. Our concern was possible fatigue failures of the aluminum, the bonding adhesive, or the actuator attachment stud.

System Reliability

With 16 actuators, the chance of a single actuator failure is *16* times as great as with a single actuator, and a single actuator failure could render the entire mirror inoperable. The entire system—actuator through surface panel-must have a high degree of reliability. Reliability was addressed by careful selection of the, actuator vendor. The vendor chosen, Industrial Drives Corporation (IDC), built 2000 actuators to drive NRAO antenna reflector panels. NRAO designed an extensive testing program, starting initially with every actuator manufacturer in the US. J} 'I, reviewed the failed actuators and the IDC prototypes. It was clear that the design and workmanship of the IDC device was superior. On that basis, IDC devices arc currently used on all deformable mirror projects.

FULL LABORATORY ASSEMBLY

The full lab assembly (shown in Figure 1) uses a 2.7-in.-diamctcr, 0.040-in.-thick aluminum plate for the deformable flat plate. The surface is controlled by 14 actuators located as shown in Figure 2. Each actuator is monitored with an LVDT attached with a flexible arm. All hardware is mounted to a base plate so that the dc.formable flat plate is only in contact with the actuators.

RESULTS TO DATE

An initial plate was constructed with only 14 of the 16 actuators shown in Figure 2. The missing actuators were the ones at the y = -11.5 inches, and y = 1 I. S-inch posit ion. This was the original output of the analysis for actuator placement optim izat ion rout inc and was based upon the desire to correct a typical reflctor distortion pat tern derived from measured surface data.[4] Using the desired surface, which is calculated to correct the RF pattern, and the predicted surface from the analysis an RMS surface deviation of ().003 in RMS was anticipated.

The actual plate (using the predicted actuator locations) was measured to be 0.032-in. RMS, a significant error. Examining the contour indicated that there were significant deviations along the plus and minus y axis, hence the addition of the two additional actuators. Using the 16 actuator plate, the (predicted-desired) surface RMS error was 0.003 in. and the (desired measured) RMS error was 0.007 in. The predicted and measrued contours arc shown in Figure 3. 'ibis is the level of RMS surface error that is necessary to achieve the necessary RF performance improvement.

FUTURE WORK

The results from the two-station device indicated that the components selected to assemble. the full DFP were reliable and cost effective. A 16-actuator DFP was assembled and tested with results that indicated the DFP would meet the RF performance improvement objectives. Using the measured plate deformation and actuator forces, the analytical model used in the optimization routine can be adjusted to more accurately represent the system. Once the difference in predicted and measured results arc reduced, the actuator placement for the 34-m BWG antenna 1 DFP will be calculated. "J he placement pattern for the antenna is expected to differ from that of the initial assembly for two reasons. First, the antenna DFP will be installed at a 30° angle so the combination of compensating for the desired contour along with gravitational loading of the plate itself will alter the overall shape. Secondly, as the antenna reflector travels in elevation, the DFP requirements will change so the actuator placement will be optimized for a family of contours rather than a single contour. The completed assembly will be installed in the 34-meter BWG antenna and antenna performance measurements will bc made. to assess the DFP cent ribution. Upon complet ion, effort wi] I be directed toward installing a DFP on the 70-meter ante.rma.

ACKNOWLEDGEMENT

The work described in this paper was carried out at the Jet Propulsion Laboratory, California Institute of Technology, under a contract with the National Aeronautics and Space Administration.

REFERENCES

[1] D. J. Rochblatt, "A Microwave holography Methodology for Diagnostics and Performance Improvement for Large Reflector Antennas," *TDA Pregress Report* 42-108, Jet Propulsion Laboratory, Pasadena, California, pp. 235-252, February 15, 1992.

[2] W. A. Imbriale, M. Moore, D. J. Rochblatt, and W. Veruttipong, "Compensation of Gravity-Induced Structural Deformations on a Beam-Wavcguidc Antenna Using a Deformable Mirror," 1995 *IEEE Antennas and Propagation Society International Symposium,* pp. 1680– 1683, Newport Beach, California, June 1995.

[3] F. Kirkpatrick, C. D. Getlatt, Jr., and M. P. Vecchi, "Optimization by Simulated Annealing," Science, vol. 220, no. 4598, May 13, 1983.

[4] F. Kirkpatrick, "Optimization by Simulated Annealing: Quantative Studies," ***Journal of Statistical Physics, vol. 34,*** no. 5/6, 1984.

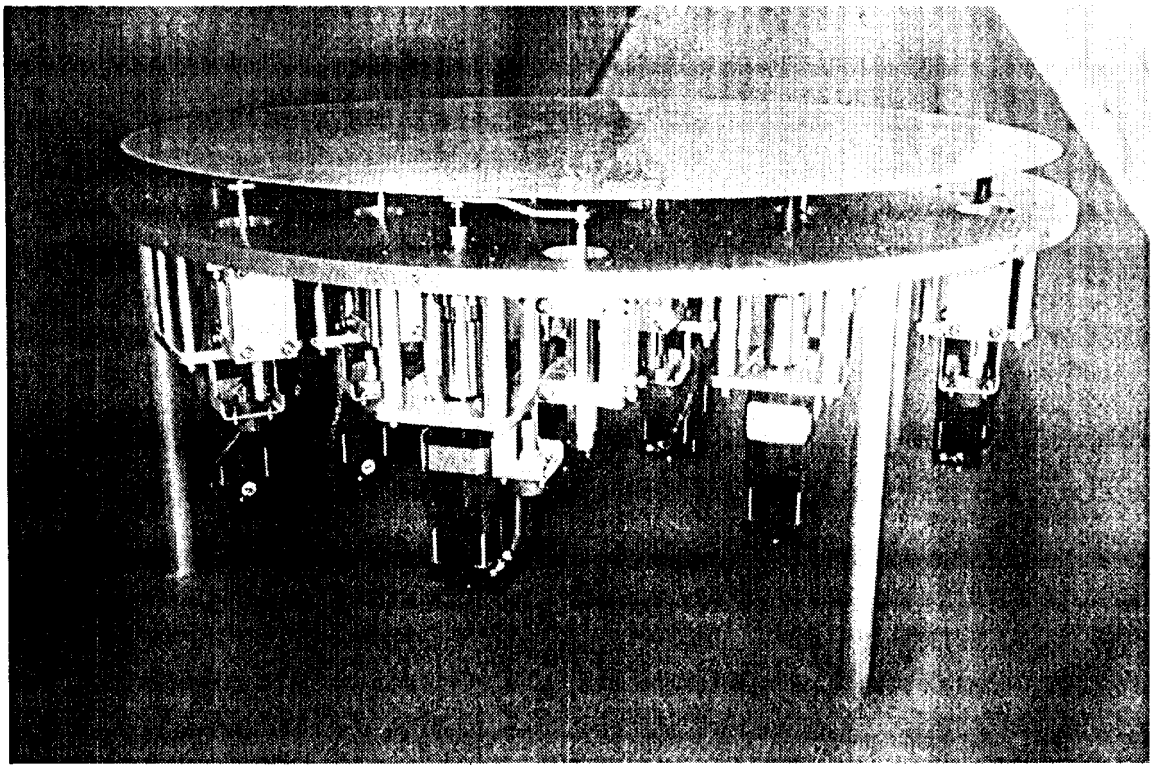

Figure 1. Full Laboratory Assembly

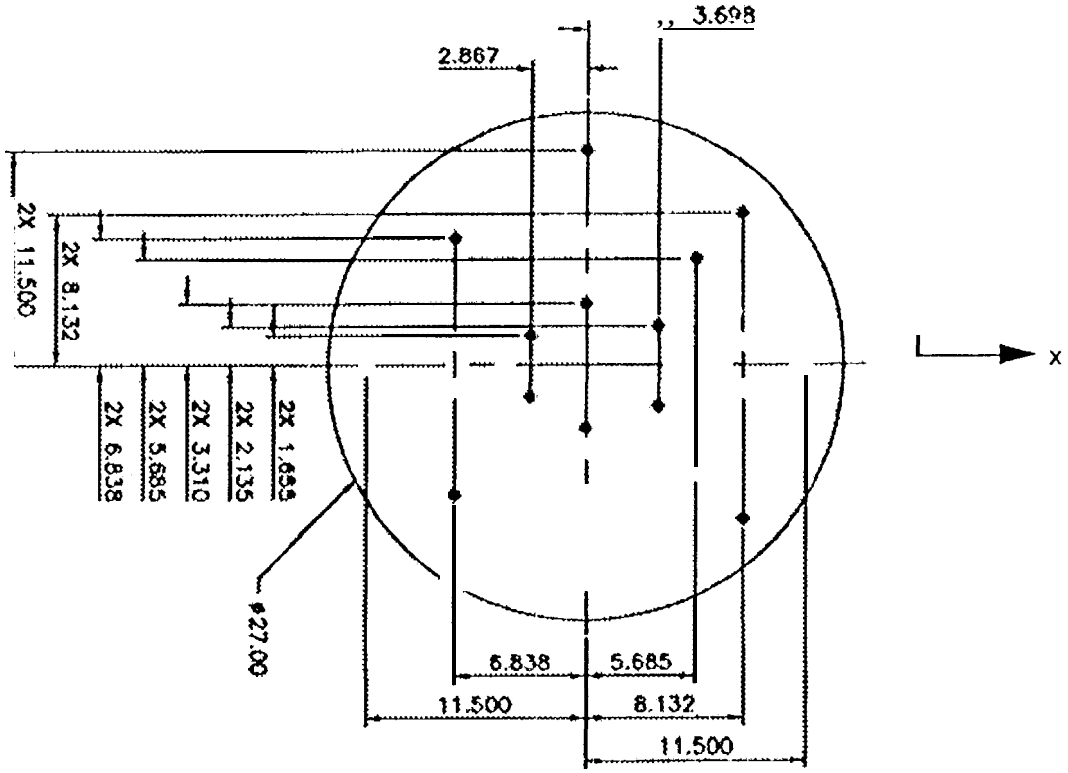

Figure 2. Actuator Locations (inches)

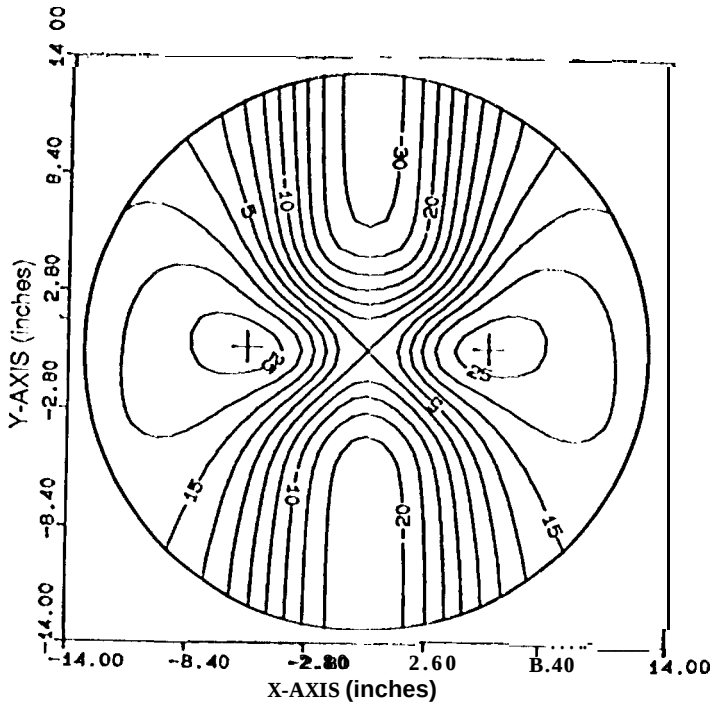

Figure 3a. Predicted Surface (Contours in roils)

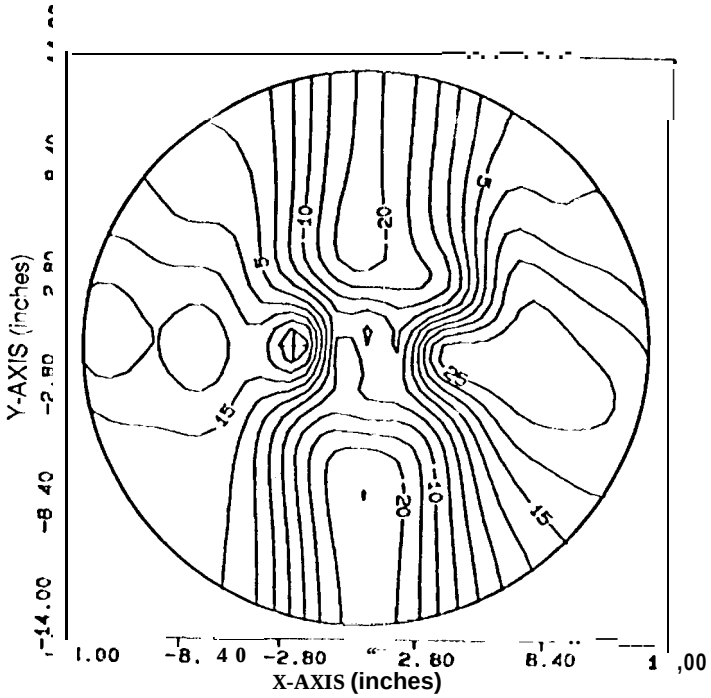

Figure 3b. Measured Surface (Contours in roils)

Figure 3. Surface that Corrects for 12.5-Degree-Elevation Angle in the 34-m Antenna